Gouveia, F., Viana da Fonseca, A., Carrilho Gomes, R., Teves-Costa, P. (2018). Deeper Vs profile constraining the dispersion curve with the ellipticity curve: a case study in Lower Tagus Valley, Portugal. Soil Dynamics and Earthquake Engineering, 109, DOI: 10.1016/j.soildyn.2018.03.010

Deeper V_s profile constraining the dispersion curve with the ellipticity curve: a case study in Lower Tagus Valley, Portugal

Fátima Gouveia (1), António Viana da Fonseca (2)

Rui Carrilho Gomes (3)

Paula Teves-Costa (4)

(1) FEUP researcher under Liquefact project

(2) CONSTRUCTGEO, Faculdade de Engenharia da Universidade do Porto

(3) CERIS, Instituto Superior Técnico, Universidade de Lisboa

(4) Instituto D. Luiz, Faculdade de Ciências, Universidade de Lisboa

ABSTRACT

Shear wave velocity profile and bedrock depth are key parameters for seismic site response estimation and a reliable tool to evaluate liquefaction potential in soil deposits. They can be determined using in-situ geotechnical tests such as the seismic Cross-Hole (CH), seismic Cone Penetration Test (SCPT), seismic Dilatometer Test (SDMT), or through geophysical surface wave methods. The main advantages of surface wave methods are their non-invasive nature and the ability to characterize the shear wave velocity of the soil at a larger scale. However, the investigation depth in general is less than 20 m. Using the Rayleigh ellipticity curve to constrain the dispersion curve from active and/or passive measurements, deeper Vs-profile is obtained.

In this study, the V_s profile of the soil at a site located over Lower Tagus alluvial Valley was obtained using different surface wave methods. For this purpose, ambient vibration measurements using a single three-component seismic station were made, to complement active and passive linear measurements. The Rayleigh wave ellipticity curve was computed from the single station recordings using the RayDec method and dispersion curves were estimated with the array recordings processed using *f-k* based methods: MASW, ReMi and conventional f-k method for non-linear array data. A joint inversion procedure was applied to the data and the results were compared with V_s profiles obtained from direct measurements with Cross-Hole and SDMT tests. The results show that considering the passive ellipticity curve in the joint inversion process with the dispersion curve, it is possible to obtain deeper and less scattered V_s profiles.

Keywords: shear-wave velocity profile, Rayleigh wave ellipticity, MASW method, passive array measurements, joint inversion.

1. Introduction

Surface wave methods are nowadays a competitive solution for the identification of shear-wave velocity profiles of the soil (Foti *et al*., 2014). These methods are used to characterize dynamic properties of the soil. For example, the HVSR method (Nakamura, 1989,2000) is used to assess the fundamental frequency of soil deposits, while the MASW (Multichannel Analysis of Surface Waves) is used to obtain the shear wave velocity profile at a large scale (Lai et al., 2002) in a non-invasive way once they do not imply the execution of boreholes. These methods use records of vibrations measured at the surface, generated by a controlled source (active) or by ambient vibration sources (passive). The resolution of the results and investigation depths depend on several parameters, such as the test setup, equipment, sources and correlation between the recorded events. Active measurements provide in general information at higher frequencies and thus about the shallow layers, while passive measurements are rich in low-frequencies, reaching deeper horizons.

There are different types of array methods that can be used to determine the dispersion curve and those are mainly divided into two groups: i) frequency-wavenumber (f-k) based methods (Capon, 1969; Lacoss et al., 1969) and ii) spatial autocorrelation based methods (Aki, 1957; Bettig et al., 2003; Gabriels et al., 1987). The MASW method (Foti, 2000; Park et al., 1999) is an f-k based method, mainly known as a linear active method. One of its main advantages, when compared to refraction methods, is that it allows identifying low velocity zones (LVZ), i.e. profiles with velocity inversions in depth.

The ReMi (Refraction Microtremor) method (Louie, 2001) is a passive linear method that also identifies the dispersion curve in the f-k domain. It is convenient in practical terms because it can use the same array used for active measurements (MASW). However, once it is used with a linear array, it is assumed in the formulation that ambient vibration sources are isotopically distributed at all azimuths. When waves arrive obliquely to the array, the estimated apparent velocity is higher than the velocity of the medium. Non-linear arrays overcome this limitation, as they ensure a good azimuthal coverage for all arrival directions, with a large aperture to provide a good resolution and a small inter-station distance for good aliasing capabilities can be used (Wathelet et al., 2007). These data can be processed using conventional f-k methods (Kvaerna and Ringdahl, 1986; Lacoss et al., 1969), high-resolution f-k method (Capon, 1969) or using spatial autocorrelation methods (Aki, 1957; Bettig et al., 2003).

The main issue of surface wave methods is a consequence of its non-invasive nature and is known as the non-uniqueness problem of the solution (Foti et al., 2009). The inversion of the seismic data gives a set of velocity models that are compatible with the experimental data.

To exclude profiles that are not compatible with the site, the current practice consists in assessing the profiles that are compatible with available geological-geotechnical data. Furthermore, the inversion of different seismic data types, that provide additional information about the soil structure, helps to increase the accuracy of the results (Scherbaum et al., 2003; Parolai et al., 2005; Lin et al., 2012).

In this paper, the Rayleigh wave ellipticity curve identified from passive single-station measurements is used in association with the dispersion curve computed from active and/or passive measurements, through a joint inversion process. By adding information from the ellipticity curve, the number of velocity models that are compatible with all the experimental data is smaller, as the uncertainty of the results. Furthermore, by combining active and passive data, which are rich at high and low frequency range respectively, deeper profiles are obtained.

The Rayleigh wave ellipticity curve is the ratio between the horizontal and vertical component of motion, as a function of frequency. Since the ellipticity curve is tightly linked to soil structure, it can be used to determine the shear wave velocity profile of the soil, for example through a joint inversion with array seismic data (Fäh et al., 2009; Hobiger, 2011; Hobiger et al., 2013). The inversion of this curve alone provides a Vs profile with large uncertainty.

The experimental ellipticity curve was determined from three-component single-station measurements of ambient vibration using a method based on the Random Decrement Technique, known as RayDec method (Hobiger, 2011). This method identifies Rayleigh waves by summing a large number of specially tuned signal windows and the effect of Rayleigh waves is highlighted by taking into account the high correlation between the horizontal and vertical components, after applying a 90º phase shift.

The aim of this work is to evaluate the accuracy of the joint inversion of Rayleigh wave dispersion and ellipticity curves for the identification of the shear wave velocity profile of the soil at a site located in the left margin of Lower Tagus Valley (LTV). The results obtained through the surface seismic methods were compared with shear wave velocity profiles obtained with the Seismic Dilatometer test (SDMT) and the Cross-Hole (CH) test for validation purposes. The inversion of the seismic data can be classified as blind, as the available geological and geotechnical data was not used to constrain the inversion process.

The shear wave velocity profile was obtained by jointly inverting different Rayleigh wave data, namely:

i) Dispersion curve obtained from active linear measurements;

ii) Dispersion curve obtained from passive linear and circular measurements;

iii) Rayleigh wave ellipticity curve computed from passive three-component single-station measurements.

In addition, the HVSR method was used to identify the fundamental frequency of the soil deposit and thus evaluate the continuity of soil layering along the study area, condition that is necessary for the application of the array seismic methods.

It is shown that the joint inversion of the single-station data and the active array provides a reliable velocity profile that is deeper, compatible with other available geotechnical test results. In this case, the passive single-station seismic data, easily obtained and used to compute the Rayleigh wave ellipticity curve, provided rich information in the low frequency range that allowed to increase the investigation depth and reduce the uncertainty of the shear wave velocity profile. Although passive circular array measurements provide rich information at lower frequencies, it did not allow accurately identifying the position of the interface between soil and bedrock. In this case, the single-station measurement, used to compute the ellipticity curve, was important to constrain bedrock depth.

2. Location and geological setting

Under the activities of the EU H2020 LIQUEFACT project ("Assessment and mitigation of liquefaction potential across Europe: a holistic approach to protect structures / infrastructures for improved resilience to earthquake-induced liquefaction disasters"), a comprehensive ground characterization was done in the Lower Tagus Valley region, located in the densely populated and developed region of the Metropolitan Area of Lisbon, at central-western mainland Portugal (Figure 1).

The stratigraphic section across the Tagus delta-estuarine plain shown in Figure 2 describes the sedimentary infilling of a Late Pleistocene valley, incised into the Tertiary substratum (Vis et al., 2008). The late Quaternary unlithified sediments are resting here mainly on Miocene deposits.

The continental deposits (see Figure 2) are formed by coarse sand, gravelly sand and gravel, poor in fine grained inter-granular matrix, with coarser pebbly lags, organized into metre scale fining upward cycles. The unit top is probably sharp and undulate in shape and it is likely to record primary depositional morphologies.

Figure 1 – Aerial view: study area and field tests location

These continental deposits are globally fining upward, being dominated by silt and argillaceous silts, with clay and fine sand intercalation. Figure 3 shows Vs generally fluctuating between 250 and 400 m/s. The marginal marine and prodelta deposits (see Figure 2) are formed by large volumes of clay, silty clay, and loams, with mollusc bioclasts. The lower 5-6 m record a fining upward evolution, from sand to clay, resulting from true marine environments. Vs values are around 150-200 m/s (Figure 3).

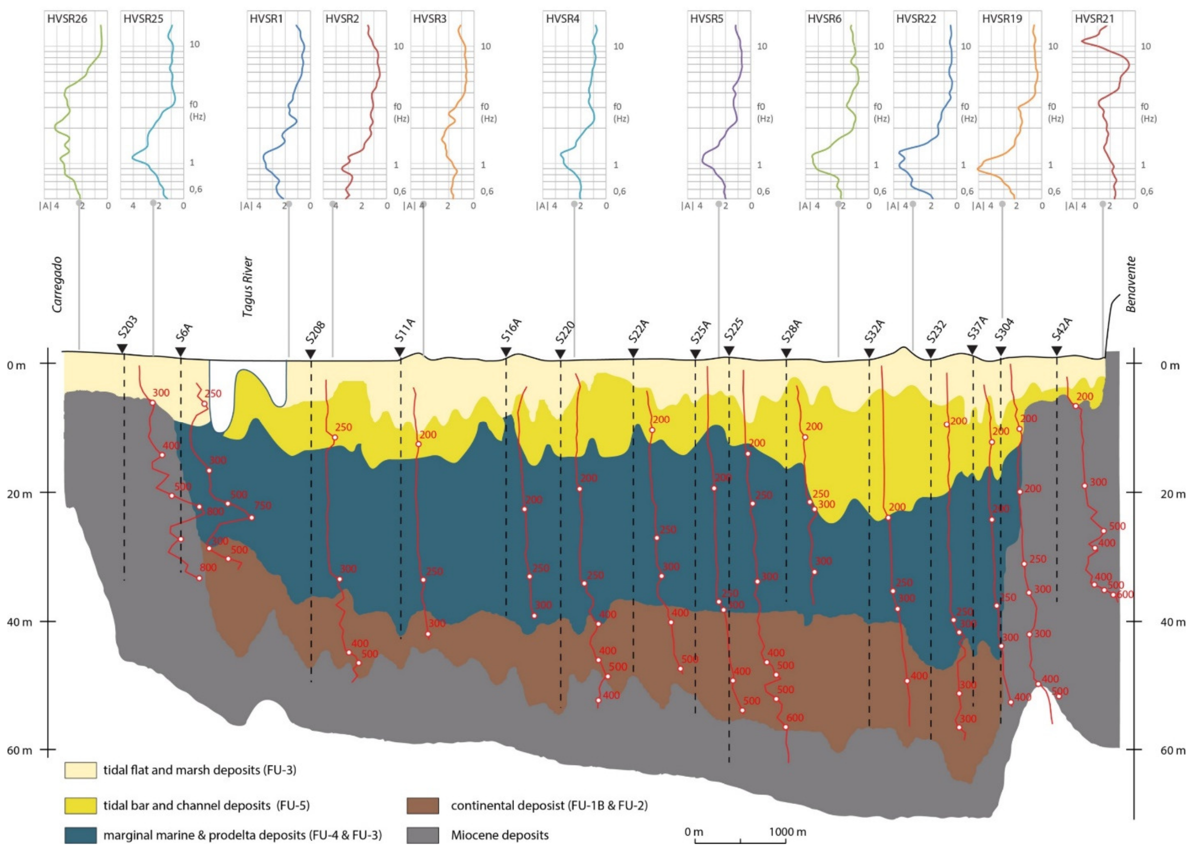

Figure 2 – Cross section along A10 bridge (see Figure 1): geology, Vs profiles from cross-hole tests and H/V curves from noise measurements (Liquefact, 2017).

The tidal bar and channel deposits (see Figure 2) consist of medium to coarse-grained sand with disturbed clay laminae in a coarsening-upward sequence. Vs fluctuate between 150 m/s and 250 m/s, with average values near 200 m/s (Figure 3).

The tidal flat and marsh deposits (see Figure 2) consist of silty clay, loam, clay, silts, with subordinated intercalation of fine grained sand, corresponding to spill over episodes. They rest on the delta-estuarine sands and are limited on the top by the topographic surface. This unit accumulated since the medieval times and was terminated by the modern land reclamation works. The unit can reach a thickness of 10 m, but it is normally just a few metres thick. The Vs profile shows the lowermost values of Vs recorded in the area, often well below 150 m/s (Figure 3).

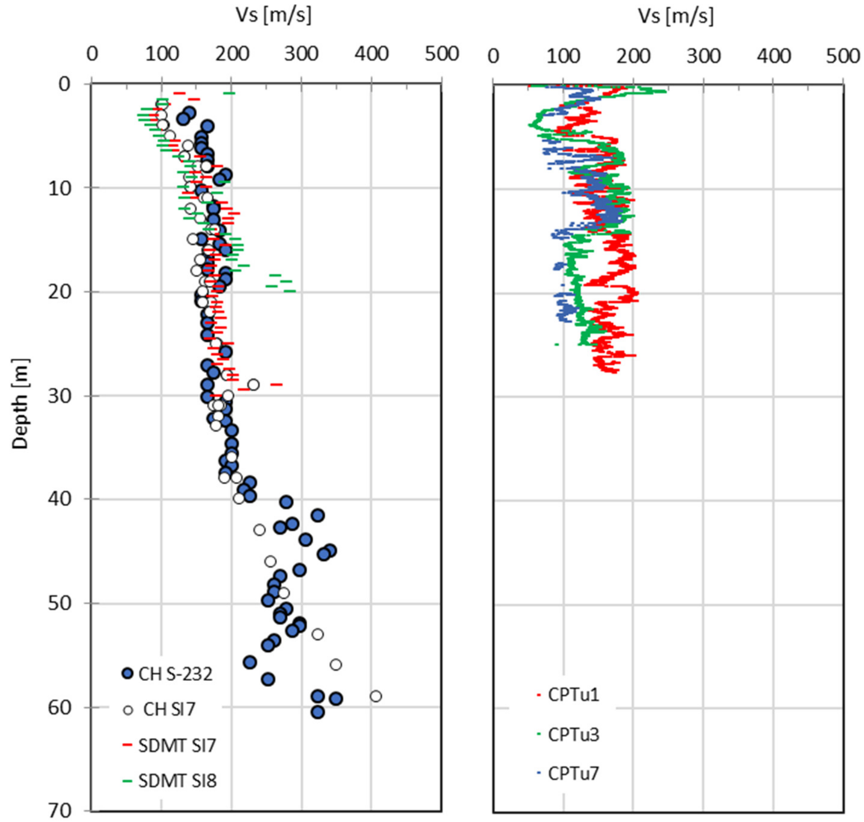

Figure 3 – Representative Vs profiles from field tests: Seismic Dilatometer (SDMT) tests, Cross-Hole (CH) tests and Cone Penetration (CPTu) tests (tests location in Figure 1)

Noise measurements were performed along the A10 cross section that crosses the central basin of the LTV (Figure 2). These measurements were processed to compute HVSR curves (Liquefact, 2017). The coupling of the Vs measurements with the HVSR curves supported preliminary considerations on the study area:

- lower frequency peaks, around 0.9-1.1 Hz, are detectable in the central basin. Those peaks may refer to the impedance contrast between the Miocene and the upper deposits, at an average depth of 50-60 m below the ground;
- higher frequency peaks, around 1.5-3.0 Hz, may be highlighted in the central basin. Those peaks may detect a shallow impedance contrast;

• higher frequency peaks, around 1.5-3.5 Hz, are visible on both borders of the basin. Those peaks may refer to the impedance contrast between the non-fractured Miocene and the upper fractured Miocene at an average depth of 7-35 m below the ground.

Recently, surface seismic refraction tests performed in the vicinity of A10 cross-section identified a shallow layer about 6 m thick with Vs around 115 m/s, overlaying a layer with Vs around 145 m/s (Carvalho *et al*., 2017).

3. Data acquisition

In this paper, to compute the dispersion curves and the Rayleigh wave ellipticity curves four types of acquisitions were done:

i) Three-component single-station ambient vibration measurements;

ii) Active-source linear array measurements;

iii) Passive linear array measurements;

iv) Passive circular array measurements.

A schematic representation of the arrays and single-station measurement points are presented in Figure 4.

Table 1 presents a summary of all the recordings made in this study, including array configuration, source distance, in case of active tests, and signal length.

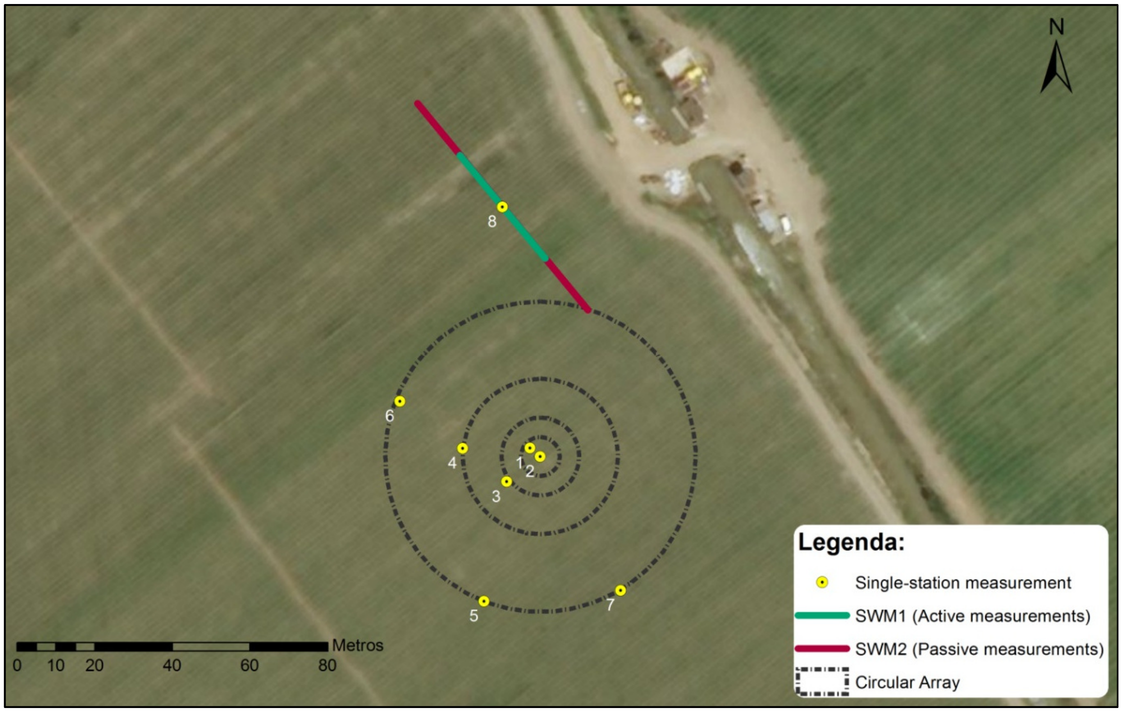

Figure 4 - Schematic representation of the arrays and single-station measurement points.

Table 1 – Characteristics of data acquisitions.

Multi-station measurements						
	Array	Source type	Sensor spacing [m]	Array length/diameter [m]	Source distance [m]	Signal length
Linear Array (vertical component)	SWM1.1	Active	1.5	34.5	3	2 s
	SWM1.2	Active	1.5	34.5	6	2 s
	SWM2	Passive	3	69	-	32 s
Circular Array (vertical component)	Ring 1	Passive		10	-	1h 40min
	Ring 2	Passive		20	-	1h 40min
	Ring 3	Passive		40	-	2h 30min
	Ring 4	Passive		80	-	2h 30min
Single-station measurements						
	Point	Source type	Location			Signal length
Single-station (three-components)		Passive	Middle of acquisition line (point 8 in Fig. 4)			30min
		Passive	Next to array receivers (points 1 to 7 in Fig. 4)			30min

Passive three-component single-station measurements:

Single-station measurements were performed using a CityShark seismic station coupled with a 3D Lennartz 1Hz seismometer. Time series were recorded during 30 min, with a sample frequency of 100 Hz and under favourable weather conditions, i.e., weak wind and no rain. The data was *detrended*, baseline corrected and 50 Hz low-pass filtered in order to avoid aliasing. In total, 8 measurements were performed, one at the middle of the linear acquisition line and 7 placed along the circular arrays (see Figure 4).

Active linear array measurements:

The active array measurements were performed using a 24-bits seismograph (RAS-24, Seistronix), connected to vertical geophones with 4.5 Hz (Geospace). The data was retrieved from 24 geophone linear spread with 1.5 m spacing (34.5 m length). Measurements were made with a sampling frequency of 100 Hz and 2 s length. The active source was a 10 kg sledge hammer hitting a steel plate. Two tests were conducted considering the source located 3 m far and 6 m far from the limit of the acquisition line. In both cases, the signal generated by the source located at each side of the acquisition line was recorded (forward and backward shots). In general, 4 recordings were made for each setup in order to allow the evaluation of the stability of the results and computation of the mean seismogram. The mean seismogram was computed by stacking all the signals, after making the corrections of the difference between arrival times due to triggering.

Passive linear array measurements:

The passive linear measurements were performed using the same equipment used for the active measurements. The line had the same orientation than the one used in active measurements, however the spacing between sensors was increased to 3 m (total length 69 m). In total, six signals were recorded with a sampling frequency of 500 Hz and during 32 s.

Passive circular array measurements:

Circular array measurements were performed using REF TEK 125A-01 Texan seismic recorder with GS-11D vertical sensors with 4.5Hz+/-0.75Hz fundamental frequency. Data were recorded with 100 Hz sampling frequency. Figure 5 shows the location of the sensors, placed as circular arrays with a central station. In total, four rings were implemented, each one composed by 8 stations, plus the central station. The ring's diameters are approximately equal to: 10m, 20m, 40m and 80m. Since only 17 stations were available, setups were done: first was placed the central station (sensor 1), Ring 1 (sensors 2 to 9) and Ring 2 (sensors 10 to 17); after was placed the central station (sensor 1), Ring 3 (sensors 18 to 25) and Ring 4 (sensors 26 to 33). The first setup (Ring 1 and Ring 2) was recorded for 1h40min and the second setup (Ring 3 and Ring 4) was recorded for 2h30min.

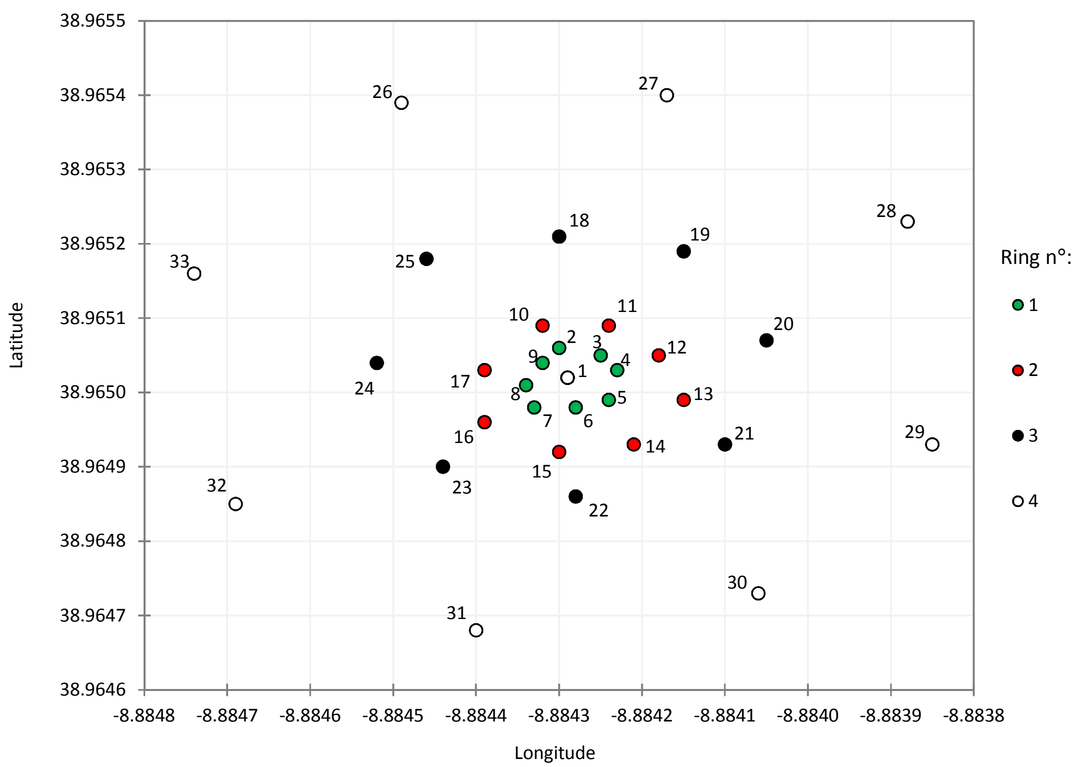

Figure 5 - Sensors distribution on the circular arrays used for passive measurements.

The resolving power of the circular arrays were evaluated through the Array Response Function (ARF), which depends on the diameter of the array, the spatial distribution of the sensors and the correlation between the events to be resolved (Wathelet et al., 2008). In this study, the ARF was determined using the *warangpds* tool from GEOPSY software (GEOPSY, 2016).

Figure 6 plots the response functions obtained by 3 different array compositions: i) Ring 1, ii) Ring 4 and iii) Ring 3 and 4. Based on this figure, the resolution and aliasing limits are defined, which are associated to the values of k_{min} and k_{max}, respectively. Results from Ring 2 are not presented because it did not add information, as discussed hereafter.

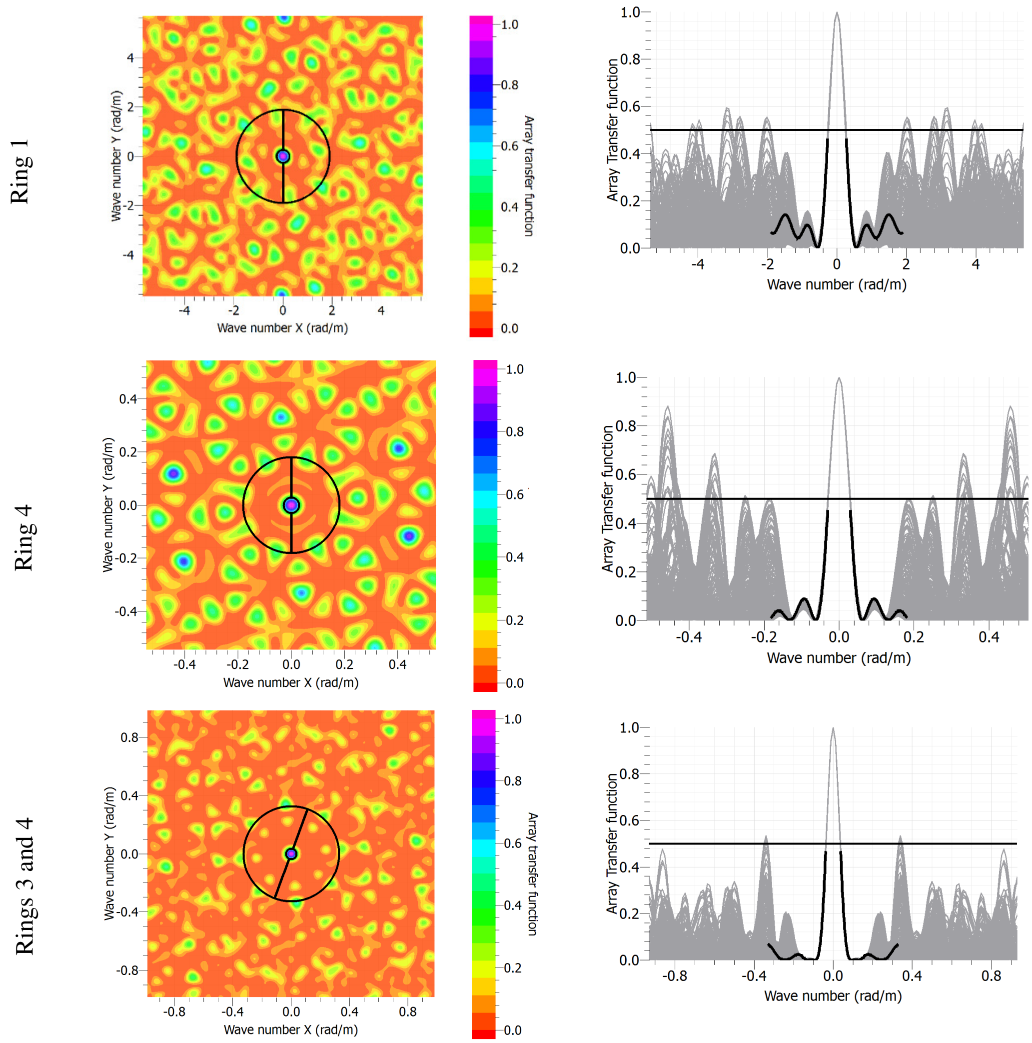

Figure 6 - Array Response Functions for arrays composed by: Ring 1, Ring 4 and Ring 3+Ring 4. Left: Wavenumber map of the ARF - circles represent the values of k_{min} *and* k_{max} *in wavenumber domain. Right: 1-D cross sections of the ARF for different azimuths, i.e., along different directions of wave propagation - the black lined is the ARF for the azimuth indicated with a black line in the wavenumber map.*

The value of k_{max} is measured at the first peak exceeding amplitude 0.5 and is mainly related to the minimum distance between sensors (D_{min}). The value of k_{min} is identified at the mid-height of the central peak and is related to the ability to identify the individual response to different waves that propagate with similar wavelength. In summary, with a higher aliasing limit, the capacity of analysis at highest frequencies increases, while with a lower resolution limit, the capacity of analysis at low frequencies decreases.

For irregular arrays, the aliasing and resolution limits depend on the array configuration and properties of the measured signal. It is recommended to keep the limits between $k_{min}/2$ and $k_{max}/2$ (Wathelet, 2005). The resolution and aliasing limits of the arrays implemented in this study are presented in Table 2.

Table 2 - Resolution and aliasing limits of the circular arrays.

						Resolution limit	Aliasing limit	λ_{max}	
	Nº stations	Station number	D_{min} [m]	D_{max} [m]	Signal length	$k_{min}/2$	$k_{max}/2$	$2\pi/(k_{min}/2)$	$3D_{max}$
Ring 1	9	1 to 9	2.7 - 4.7	10	1h40min	0.2679	0.9494	23.5	30
Ring 2	9	1 + 10 to 17	6.6 - 9.0	20		0.1215	0.4682	51.7	60
Ring 3	9	1 + 18 to 25	13.2 - 17.4	40	2h30min	0.0596	0.1828	105.4	120
Ring 4	9	1 + 26 to 33	27.7 - 34.8	80		0.0303	0.0908	207.4	240
Rings 1 and 2	17	1 to 17	2.7 - 4.7	20	1h40min	0.1535	2.7800	40.9	60
Rings 3 and 4	17	1 + 18 to 33	13.2 - 17.4	80	2h30min	0.0376	0.16447	167.1	240

The array composed by Ring 4 has the highest maximum distance between sensors (D_{max}). So, its lower resolution limit means higher capacity to analyse in the low frequency range. It is also the array that presents the higher minimum distance between sensors (D_{min}) and thus the lower aliasing limit. This means the lower capacity of analysis at highest frequencies. Comparing to the latter, the array composed by Rings 3 and 4, has higher capacity of analysis at high frequencies and slightly lower capacity of analysis at low frequencies.

The data recorded with the smaller array (Rings 1 and 2) provided frequency-velocity values that match the ones identified with active linear measurements. As different methods provide similar results, the confidence and robustness of the results is higher.

4. METHODOLOGY

4.1. HVSR method

The three-component single-station measurements of ambient vibration were used to compute the Horizontal-to-Vertical spectral ratio (HVSR) using GEOPSY software (GEOPSY, 2016). The average HVSR curve was computed based on the most stationary time windows, with 30 s length. Those were tapered with 5% cosine function. The curves were smoothed using the Konno-Ohmachi algorithm (Konno and Ohmachi, 1998), with a smoothing constant of 40.

The reliability of the identified fundamental frequency, as corresponding to the HVSR peak frequency, was verified based on the criteria proposed in SESAME guidelines (SESAME Team, 2004), including the criteria for a reliable HVSR curve and the criteria for a clear HVSR peak. The criteria for a reliable H/V curve aim to ensure that the curve is stable, by limiting i) the minimum number of significant cycles (related to the peak frequency) within each time window, ii) the minimum number of time windows used to compute the average HVSR curve and iii) the standard deviation values. The criteria for a clear HVSR peak aim to ensure that the HVSR peak is unique and sufficiently clear to assume it as corresponding to the fundamental frequency of the soil deposit. The latter criteria stablish limits for: i) the minimum amplitude of the HVSR peak and relative value with respect to HVSR peaks in other frequencies, ii) the relative value of standard deviation of amplitude and peak frequency estimated from individual time windows. In this study, several long-duration recordings were made to ensure that enough stationary signals were recorded and used to obtain a stable HVSR curve.

The HVSR method was used to evaluate the continuity of soil layering along the area where the arrays were implemented, through the comparison of the HVSR peak frequency and maximum amplitude.

4.2. Rayleigh wave ellipticity

The Rayleigh wave ellipticity curve used for the identification of the shear wave velocity profile was computed using the RayDec method (Hobiger et al., 2009; Hobiger, 2011) from the three-component single-station measurements. The average curve and standard deviation was obtained considering the ellipticity curves extracted from 6 time windows with 5 min length (30 min of total length). The two free parameters of the method, namely the length of the buffered signal (Δ) and width of the frequency filter (df) were defined as corresponding to 10/f and 0.2f, respectively.

4.3. Rayleigh wave dispersion curve

The dispersion curves were identified for all tests, using f-k based methods, i.e., i) active linear measurements (MASW method), ii) passive linear measurements (ReMi method) and iii) passive circular measurements (conventional f-k method). The active linear data and passive circular data was processed using GEOPSY software and the passive linear data was processed using SWAN software (Geostudi Astier Inc., 2007).

All the data, array and single-station data, was detrended and low-pass filtered based on the sampling frequency (f_s) to $1/2f_s$ to avoid temporal aliasing.

For the active linear measurements, the signals recorded with the same acquisition line and the same source was stacked after correcting triggering time in order to reduce the incoherent noise. The presented dispersion curves were obtained using the mean seismogram (stacked signal). Furthermore, the dispersion curves computed using signals generated with different sources (forward or backward shot) on the same acquisition line were compared to identify possible lateral variations along the line.

For the passive linear measurements, the symmetry of the f-k spectra was analysed to evaluate the validity of the hypothesis assumed in ReMi method, which states that the distribution of sources is uniform. The dispersion curves were automatically picked at points that contain 80% of the maximum energy. Once the method tends to overestimate the velocity of the medium, these dispersion curves were compared to the ones obtained with active linear measurements.

The circular array data was processed using the conventional f-k method (Kvaerna and Ringdahl, 1986), considering time windows with length that depend on the period (50.T). The grid step was defined taking into account the ARF (Array Response Function), namely based on the resolution and aliasing limits. The grid step was defined lower than $k_{min}/4$ and grid size higher than $k_{max}/2$. The bandwidth factor of the central frequency was defined as 0.10.

4.4. Joint inversion of Rayleigh wave data

The joint inversion of the dispersion and ellipticity curves was made using a modified version of the Neighbourhood Algorithm (Wathelet, 2005), implemented in *Dinver*, a tool from GEOPSY software (GEOPSY, 2016).

The velocity model was defined with four layers over half-space. The V_s value could vary between 80-500m/s for the soil layers and between 100-1500 m/s for half-space. It was only allowed velocity inversion at the second layer, since these shallow alluvial deposits may be affected by water level fluctuations as suggested by the borehole data. The values of P-wave velocity were linked to the values of V_s through the Poisson ratio, which was allowed to vary between 0.2 and 0.5. The density was kept constant and equal to 1800kg/m^3. It should be noticed that the effect of the value of Poisson's ratio and density of the medium is not significant on the dispersion and ellipticity curves.

The joint inversion process was made considering equal misfits for both data. The tuning parameters were defined to allow a good exploration of the parameter space and the inversion process was repeated to evaluate the stability of the results. In total, 401 200 models were analysed at each run.

5. RESULTS

5.1. HVSR and Rayleigh wave ellipticity

The HVSR curves obtained with all three-component single-station measurements of ambient vibration and distribution of the peak frequencies of the average HVSR curves within the circular array are presented in Figure 7. The reliability of the peak frequencies was verified for all curves, based on the criteria presented in SESAME guidelines (SESAME Team, 2004)

All measurements provide very stable shapes of the main peak. The main differences between the curves are related to the second maximum, which might be associated with a different impedance contrast or with a higher mode. The average curves presented a peak frequency between 1.00 and 1.18 Hz, within the circular array (points 1 to 7, in Figure 4) and equal to 1.15 Hz at the point located at the middle of the linear acquisition line (point 8, in Figure 4). The range of variation of the maximum amplitude is narrow, between 3.9 and 4.5. The lowest values were obtained at points 1 (Ring 1) and 3 (Ring 2) (see Figure 4), located in the central area of the circular array but, at the centre of the arrays (point 2), the amplitude was similar to the remaining curves.

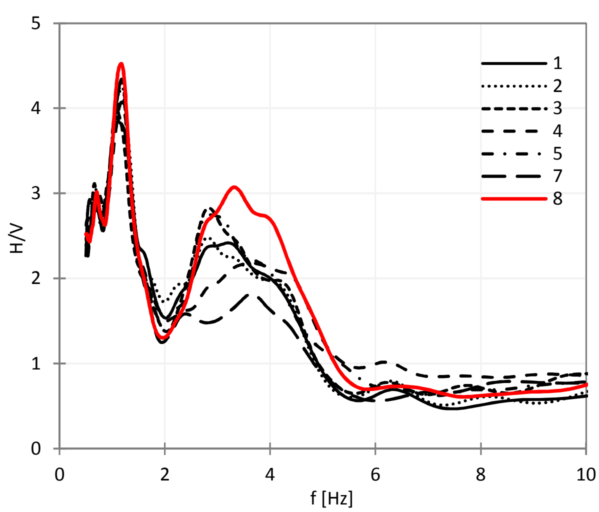

Figure 7 - Microtremor HVSR curves obtained at points within the circular array (curves 1 to 7) and at the middle of the linear acquisition line (curve 8.) See figure 4 for point locations)

Since the difference in frequency and amplitude are small, no significant variations in the soil profile along the study area are expected, including the impedance contrast between soil and bedrock. This conclusion is compatible with the available information about local geology.

The Rayleigh wave ellipticity curve and HVSR curve computed using the measurement performed at the middle of the linear acquisition line, as well as the peak frequency value, are presented in Figure 8. In general, the ellipticity curve follows the shape of the HVSR curve. The peak amplitude of both curves is relatively close, which suggests that Rayleigh waves have a major contribution to the measured wave field.

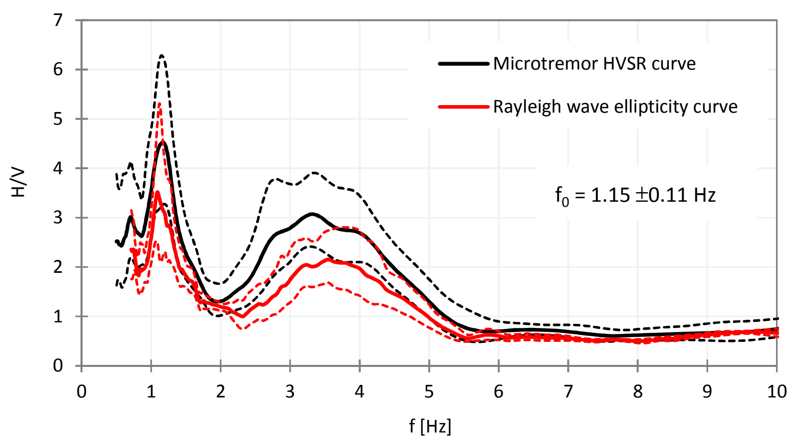

Figure 8 – Microtremor HVSR curve and ellipticity curve obtained with recording made at the middle of the linear array.

5.2. Rayleigh wave dispersion curve

In this section, the Rayleigh wave dispersion curves from active and passive acquisitions are analysed.

The dispersion curves from linear active measurements are very stable and the identification of the fundamental mode is clear (Figure 9). The lateral variation along the acquisition line is negligible because the dispersion curves from the forward and backward shots are similar.

The dispersion curves obtained with SWM1.1 (3m source distance) and SWM1.2 (6m source distance and 34.5 m length) are identical and, in this case, no gain was obtained by changing the source distance.

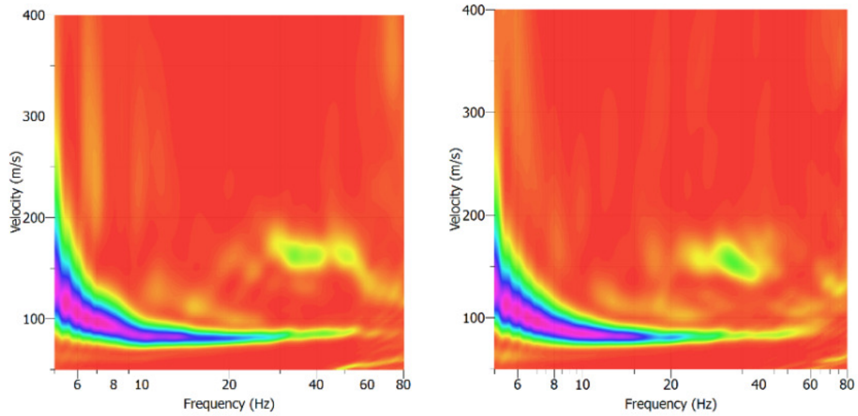

Forward shot Backward shot

Figure 9 - V-f spectra obtained with active recordings made with SWM1.1 (3m source distance).

The identification of the dispersion curve derived from passive linear measurements (ReMi method) is not so clear. This is because a high variation of the energy distribution is identified in the f-k domain, as exemplified in Figure 10 for SWM2 (69m length) record. In this Figure, the spectra are clearly asymmetric, which indicates that ambient vibration sources are not isotropically distributed in all azimuths. Once the hypothesis of uniform distribution of the sources is assumed in the formulation of ReMi method, its application for the identification of the dispersion curve may not be appropriate.

In general, the f-k spectra present scattered energy (ex.: recording Lez0122), however in some records (e.g. Lez0116 and Lez0119) non-uniform source distribution can be identified (see Figure 10). In those cases, the dispersion curve was extracted by picking the points next to the maximum energy points.

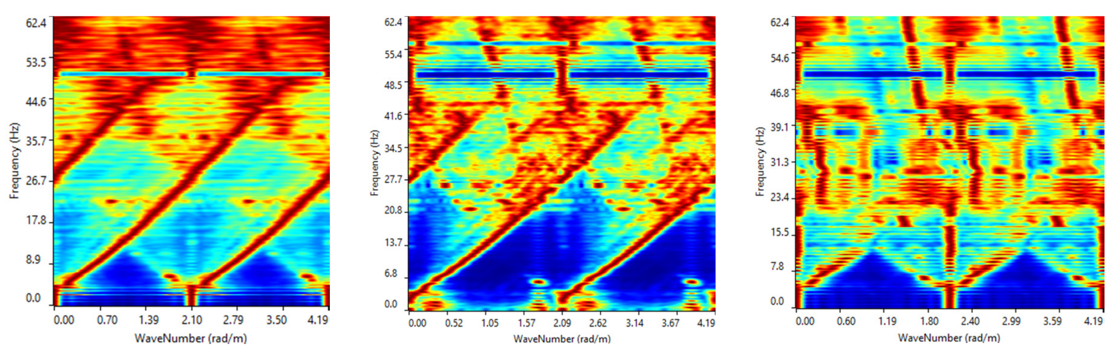

(Lez0116) (Lez0119) (Lez0122)

Figure 10 –Frequency-wavenumber spectra computed using the passive linear measurements.

The circular array data was processed with the data acquired at Rings 3 and 4. This option was taken because comparing with Ring 4 (Figure 6), these two Rings, 3 and 4, have higher capacity of analysis at high frequencies, without losing relevant information in the low frequency range.

Figure 11 plots the dispersion curves obtained from all active and passive measurements. All the curves are very well adjusted, showing the stability of the results and proving that there are no significant lateral variations in the study area.

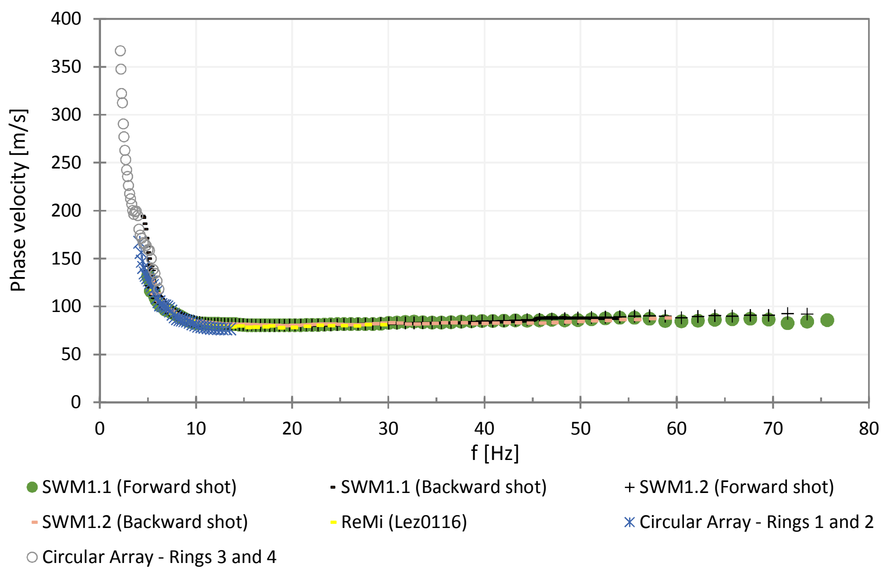

Figure 11 - Dispersion curves computed using the active and passive measurements.

In this case, the passive linear array data was able to identify the correct value of velocity with the ReMi method, although the presence of a non-uniform wave field. Both active and passive linear arrays provide information above about 4.5 Hz. While the passive linear array provides information up to 30 Hz, the active linear array goes above 70 Hz.

The passive circular array (Rings 3 and 4) provide relevant information at very low frequency range, approximately up to 2 Hz. However, since the sensors used have fundamental frequency of 4.5Hz+/-0.75 Hz, values below 4.0 Hz were not considered in the inversion, because the response of the sensor at lower frequencies is attenuated.

5.3. Shear wave velocity profile

In this study, the shear wave velocity profile of the soil was identified through the inversion of the dispersion curve alone and through the joint inversion of the dispersion curve and ellipticity curve computed using the measurement performed at the middle of the active acquisition line (point 8, Figure 4).

As all the dispersion curves presented in Figure 11 are similar and nearly overlapped, the dispersion curve that was considered in the inversion contains information obtained with: i) active measurements performed with SWM1.1 (Forward shot) for f > 6.0Hz, because it contains more information at high frequencies and the curve is quite regular, and ii) passive circular array measurements for 4.0 < f < 6.0Hz, including its standard deviations.

Concerning the Rayleigh wave ellipticity curve, since it presents a well-defined peak, both left and right sides of the curve were inverted because it helps in constraining the peak frequency (Gouveia, 2017; Hobiger et al., 2013).

The inversion results obtained by considering the dispersion curve alone, are presented in Figure 12. The correspondent velocity models plotted have a misfit lower than 2×min. misfit.

With the inversion of the dispersion curve alone, a 20 m deep shear wave velocity profile of the soil was obtained, presenting high uncertainty for higher depths. In general the velocity increases with depth, however a small reduction of velocity was identified at the second layer (velocity inversion). The identified models present a shallow velocity of 90-100m/s up to 6 m deep, followed by a layer with 200 m/s until at least 20 m depth.

The results obtained through the joint inversion of the dispersion curve and both left and right sides of the ellipticity curve are presented in Figure 13. Those velocity models are associated with a misfit lower than 1.3×min. misfit.

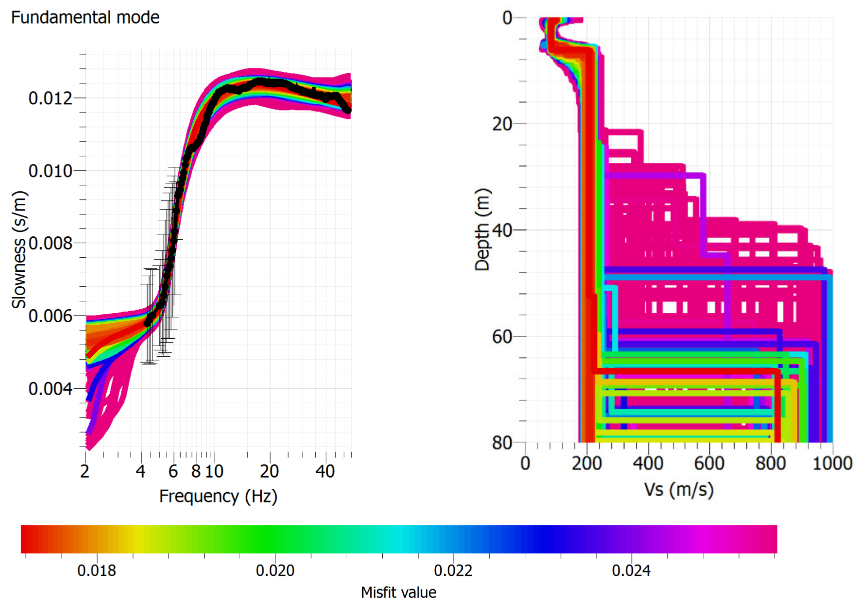

Figure 12 - Inversion of the dispersion curve alone.

The shallow part of the shear wave model is similar to the one obtained with the inversion of the dispersion curve alone, i.e., a shallow layer with approximately 90 m/s until 6 m depth, followed by a stiffer layer with 190-210 m/s. However, by adding the information obtained from the single-station measurements, it is possible to identify the approximate location of the interface between the soil deposit and the Miocene formation (around 48-60 m depth) and velocity of the latter unit, which is estimated between 520-590 m/s. Therefore, it can be concluded that the dispersion curve is responsible for fixing the V_s values at shallow layers, and the ellipticity curve can be used to reduce the uncertainty of deeper layers and adjust the depth of the interface with half-space.

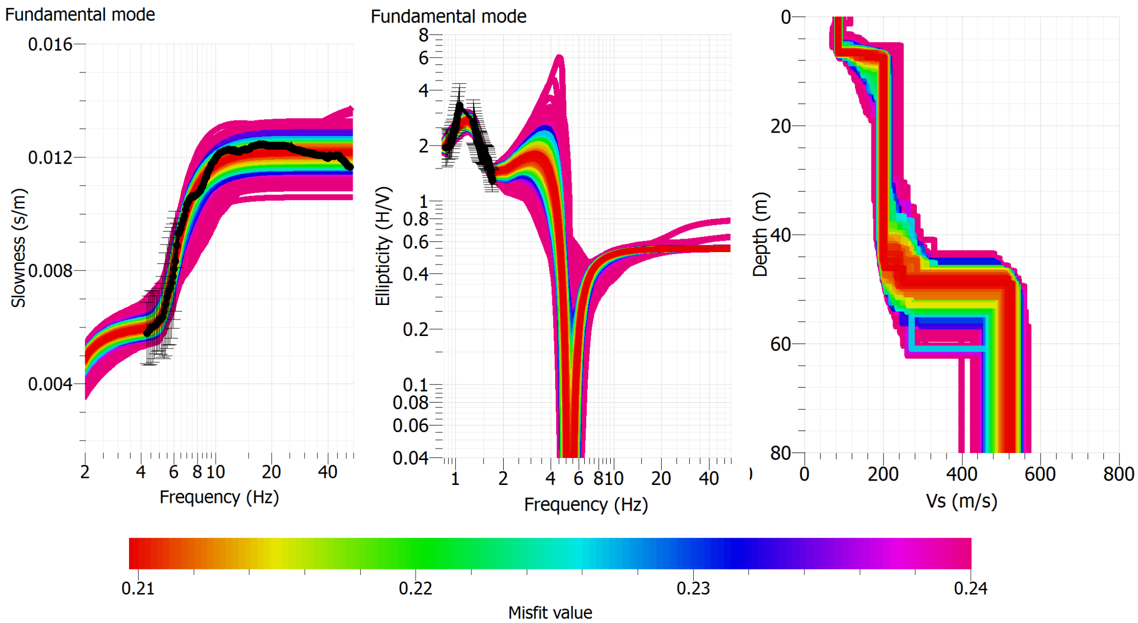

Figure 13 - Joint inversion of Rayleigh wave dispersion and ellipticity curves.

5.4. Discussion of the results

The inversion of the dispersion curve obtained from active linear measurements and passive circular array measurements allowed to obtain a relatively deep shear wave velocity profile. However it was not enough to accurately identify the position of the interface between the soil deposit and the bedrock (Figure 12) because the uncertainty at depths higher than 25m is high.

By adding the information extracted from the three-component single-station measurements of ambient vibration, namely the Rayleigh wave ellipticity curve, it was possible to better constrain of the position of this soil/bedrock interface. In fact, the variation of the velocity values and thickness of the layers of the Vs profiles obtained has been greatly reduced at higher depths (Figure 13), when compared to the one shown in Figure 12.

The evaluation of the reliability of the results was made by analysing the compatibility between the set of velocity models with (i) the experimental seismic data and (ii) the available shear wave velocity profiles obtained in previous studies from CH and SDMT tests.

The HVSR peak frequency values obtained in all three-component single-station measurements of ambient vibration vary between 1.00-1.18Hz, which may correspond to the fundamental frequency of the soil deposit at the points where the measurements were performed. These values are within the expected peak frequency values identified in previous site effect studies performed in the central basin of the LVT (Vis et al., 2008; Vis et al., 2016; Liquefact, 2017).

Taking into account the Vs models presented in Figure 13, the average shear wave velocity, Vs, can be taken equal to ~200m/s up to a depth of about 50 m (H). Assuming the vertical propagation of shear waves in visco-elastic layer, the fundamental frequency, f_0, can be estimated by the ratio between Vs and 4H. Thus, f0 is equal to ~1.00 Hz, which is compatible with the frequency of the peaks observed in HVSR curves (Figure 7).

It is very complex to evaluate with precision the compatibility between the amplitude of the HVSR experimental curves (Figure 7) and the velocity models obtained through the inversion process. As referred in Section 1, modelling the experimental HVSR curve is very complex, because it is necessary to know previously the composition of the measured wave field. Unfortunately, the composition of the wave field is not known. In the case in analysis, the compatibility between the experimental HVSR curve and the velocity profiles was done qualitatively, addressing specially the peak amplitude.

The shear wave velocity profiles presented in Figure 13 were obtained by inverting both dispersion and ellipticity curves. Because the fundamental mode of the ellipticity curve is well adjusted, it can be concluded that the theoretical HVSR curves associated to those velocity profiles are compatible with the experimental HVSR curves, at least for its peak frequency. It should be noted that, when high impedance contrast between soil and bedrock exists, the peak frequency of the experimental HVSR curve is very close to the peak frequency of the Rayleigh wave ellipticity curve. In this case, the ellipticity peak of the resultant velocity models is around 1.1-1.2 Hz and the HVSR peak frequency of the experimental curve (Figure 8) is equal to 1.15 Hz.

The evaluation of the compatibility between the velocity models and the peak amplitude of the HVSR curve is more complex. Although both HVSR curve and Rayleigh wave ellipticity curve are defined as the spectral ratio between the horizontal and vertical components of motion, the amplitude of the experimental ellipticity curve is always lower than the peak amplitude of the HVSR curve. This occurs because the HVSR curve contains the effect of other waves besides Rayleigh waves, such as Love waves, that increase the HVSR ratio.

In this case, the experimental HVSR curves showed a peak amplitude between 3.8 and 4.5 (Figure 7) and the calculated average ellipticity curve presents a peak amplitude of 2.8-3.4 (Figure 8). The velocity models obtained through the joint inversion process were well adjusted to the estimated experimental ellipticity curve, presenting a peak amplitude between 2.6 and 3.2 (Figure 13).

Figure 14 plots the results obtained through the joint inversion process with the available velocity profiles obtained with Seismic Cross-Hole (CH) and Dilatometer (SDMT) tests near the study area (see Figures 1 and Figure 3). It can be verified the compatibility of the velocity models, in terms of velocity values and location of the interface between the soil deposit and the Miocene formation 50-60 m deep. Also, the seismic refraction test results (Carvalho et al., 2017) are compatible with the Vs profile from joint inversion, namely a shallow layer about 6 m thick with Vs around 115 m/s, overlaying a layer with Vs around 145 m/s.

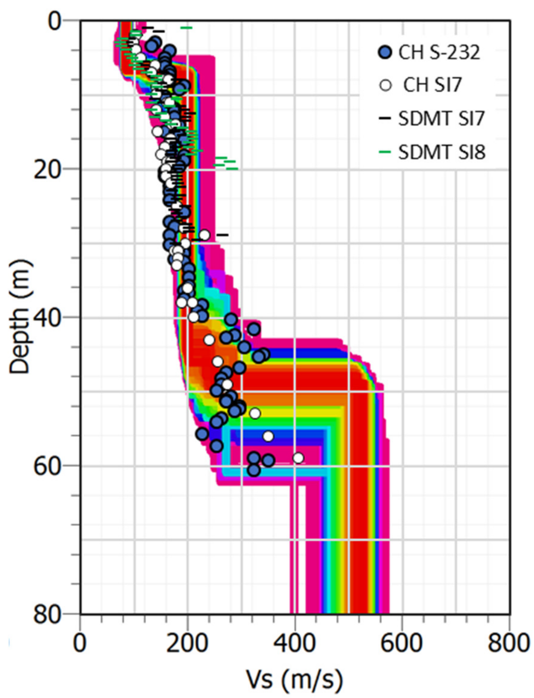

Figure 14 – Comparison between the shear wave velocity profiles obtained through the joint inversion process and through Cross-Hole (CH) and Seismic Dilatometer (SDMT) tests.

6. FINAL REMARKS

In this study, the shear wave velocity profile of a site located in LTV was identified using surface wave methods. For this purpose, four types of acquisitions were performed: active and passive linear measurements, passive circular measurements and three-component single-station measurements of ambient vibrations. The V_s profile was identified through the inversion of the dispersion curve alone, computed using active and passive array measurements, and also through the joint inversion of the dispersion curve and the Rayleigh wave ellipticity curve. This ellipticity curve was used to constrain the Vs profile in the low frequency range, increasing the depth of the profile with low uncertainty.

Although in this case the soil structure is relatively simple, no significant variation of bedrock depth is expected and there was enough space available to implement wide circular arrays, it was not possible to accurately identify the V_s profile until the bedrock using only array methods.

It can be concluded that the use of the passive three-component single-station data, which is very simple to obtain, in addition to the array data, allowed to significantly increase the resolution of the velocity profile at higher depths (from about 25 m to around 50 m) and reduce the uncertainty of the results. It should be noted that this technique is especially useful to characterise areas with space limitations, such as urban areas. If long arrays cannot be implemented to collect low frequency content information, the characterisation of deeper layers is not possible. The velocity models obtained through the joint inversion process are in good agreement with profiles obtained from invasive seismic tests as Seismic Cross-Hole, Dilatometer and refraction tests

Acknowledgements

LIQUEFACT project ("Assessment and mitigation of liquefaction potential across Europe: a holistic approach to protect structures / infrastructures for improved resilience to earthquake-induced liquefaction disasters") has received funding from the European Union's Horizon 2020 research and innovation programme under grant agreement No GAP-700748

The authors would like to express their thanks to Dr. Luca Minarelli for the cross section along A10 bridge (Figure 3).

REFERENCES

Aki, K. (1957). Space and Time Spectra of Stationary Stochastic Waves, with Special Reference to Microtremors. Bull. Earthquake Res. Inst. Tokyo Univ.

Bettig, B., Bard, P.-Y., Scherbaum, F., Riepl, J., Cotton, F., Cornou, C., & Hatzfeld, D. (2003). Analysis of dense array measurements using the modified spatial auto-correlation method (SPAC). Application to Grenoble area. Bolletino Di Geofisica Teorica Ed Applicata, 42(3–4), 281–304.

Carvalho, J., Dias, R., Filipe, A., Leote, J., (2017). Report on the works of seismic refraction performed at Lezíria between Vila Franca de Xira and Benavente for the computation of propagation velocity of P and S seismic waves. LNEG, Lisbon, Portugal. (in portuguese)

Capon, J. (1969). High-Resolution Frequency-Wavenumber Spectrum Analysis. IEEE, 8, 1408–1419.

Fäh, D., Wathelet, M., Kristekova, M., Havenith, H.-B., Endrun, B., Stamm, G., Poggi, V., Burjanek, J. & Cornou, C. (2009). Using Ellipticity Information for Site Characterisation Using Ellipticity Information for Site Characterisation. Technical report, NERIES JRA4-D4, Task B2, 54pp.

Foti, S., Lai, C.G., Rix, G.J., Strobbia, C., (2014). Surface Wave Methods for Near-Surface Site Characterization. CRC Press, 487 Pages, ISBN 9780415678766-

Foti, S. (2000). Multistation Methods for Geotechnical Characterization using Surface Waves. Politecnico di Torino.

Foti, S., Comina, C., Boiero, D., & Socco, L. V. (2009). Non-uniqueness in surface-wave inversion and consequences on seismic site response analyses. Soil Dynamics and Earthquake Engineering, 29(6), 982–993.

Gabriels, P., Snieder, R., & Nolet, G. (1987). In situ measurements of shear-wave velocity in sediments with higher-mode Rayleigh waves. Geophysical Prospecting, 35, 187–196.

GEOPSY (2016). http://www.geopsy.org/. Retrieved from http://www.geopsy.org/

Geostudi Astier Inc. (2007). SWAN - Surface waves analysis. Italy (http://www.geostudiastier.it).

Gouveia, F. (2017). Dynamic characterization of the soil in urban areas under confined conditions. PhD

Thesis, Instituto Superior Técnico, University of Lisbon.

Hobiger, M., (2011). Polarization of surface waves: characterization, inversion and application to seismic hazard assessment. Earth Sciences. Universite Grenoble Alpes, 2011. English.

Hobiger, M., Bard, P.-Y., Cornou, C. & Le Bihan, N. (2009). Single station determination of Rayleigh wave ellipticity by using the random decrement technique (RayDec). Geophysical Research Letters, 36(14), L14303.

Hobiger, M., Cécile, C., Wathelet, M., Di Giulio, G., Knapmeyer-Endrun, B., Renalier, F., Bard, P.-Y., Savvaidis, A., Hailemikael, S., Le Bihan, N., Ohrnberger, M., Theodoulidis, N. (2013). Ground structure imaging by inversions of Rayleigh wave ellipticity : sensitivity analysis and application to European strong-motion sites. Geophysical Journal International, 192 (1), 207-229.

Konno, K., & Ohmachi, T. (1998). Ground-Motion Characteristics Estimated from Spectral Ratio between Horizontal and Vertical Components of Microtremor. Bulletin of the Seismological Society of America, 88(1), 228–241.

Kvaerna, T., & Ringdahl, F. (1986). Stability of various fk-estimation techniques. In Semiannual Technical Summary. NORSAR Scientific Report 1-86/87 (pp. 29–40). Kjeller, Norway.

Lacoss, R. T., Kelly, E. J., & Toksoz, M. N. (1969). Estimation of seismic noise structure using arrays. Geophysics, 34(1), 21–38.

Lai, C. G., Rix, G. J., Foti, S., & Roma, V. (2002). Simultaneous measurement and inversion of surface wave dispersion and attenuation curves. Soil Dynamics and Earthquake Engineering, 22(9–12), 923–930.

Lin, F-C., Schmandt, B., Tsai, C.V. (2012). Joint inversion of Rayleigh wave phase velocity and ellipticity using USArray: Constraining velocity and density structure in the upper crust. Geophysical Research Letters, 39 (12).

Liquefact (2017) - Assessment and mitigation of Liquefaction potential across Europe: a holistic approach to protect structures/infrastructure for improved resilience to induced Liquefaction disasters. (H2020-DRA-2015, GA no. 700748) - DELIVERABLE D2.1 - Report on ground characterization of the four areas selected as testing sites by using novel technique and advances methodologies to perform in situ and laboratory tests (http://www.liquefact.eu/).

Louie, J. N. (2001). Faster, better: Shear-wave velocity to 100 meters depth from refraction microtremor arrays. Bulletin of the Seismological Society of America, 91(2), 347–364.

Nakamura, Y. (1989). A Method for Dynamic Characteristics Estimation of Subsurface Using Microtremor on the Ground Surface. Quarterly Report Railway Technical Research Institute, Tokyo, 30, 25–33.

Nakamura, Y. (2000). Clear identification of fundamental idea of Nakamura's technique and its applications. In Proceedings of the 12th World Conference on Earthquake Engineering. Auckland.

Park, C. B., Miller, R. D., & Xia, J. (1999). Multichannel analysis of surface waves. Geophysics, 64(3), 800–808.

Parolai, S., Picozzi, M., Richwalski, S.M., Milkereit, C. (2005). Joint inversion of phase velocity dispersion and H/V ratio curves from seismic noise recordings using a genetic algorithm, considering higher modes. Geophysical Research Letters, 32 (1).

SESAME Team. (2004). Guidelines for the implementation of the H/V spectral ratio technique on ambient vibrations - Measurements, processing and interpretation. SESAME European Research Project, WP12 - Deliverable D23.12, 1–62.

Scherbaum, F., Hinzen, K.-G., Ohrnberger, M. (2003). Determination of shallow shear wave velocity profiles in the Cologne, Germany area using ambient vibrations. Geophysical Journal International 152(3), 597–612.

Vis G-J, Kasse C and Vandenberghe J (2008) Late Pleistocene and Holocene paleogeography of the Lower Tagus Valley (Portugal): effects of relative sea level, valley morphology and sediment supply. Quat. Sci. Rev. 27(17–18): 1682–1709.

Vis G-J, Kasse C, Kroon D, Vandenberghe J, Jung S, Lebreiro S and Rodrigues T (2016) Time-integrated 3D approach of late Quaternary sediment-depocenter migration in the Tagus depositional system: From river valley to abyssal plain. Earth-Science Reviews. 153: 192-211

Wathelet, M. (2005). Array recordings of ambient vibrations: surface-wave inversion. PhD Thesis. University of Liège, Belgium.

Wathelet, M., Jongmans, D., Ohrnberger, M., & Bonnefoy-Claudet, S. (2007). Array performances for ambient vibrations on a shallow structure and consequences over V s inversion. Journal of Seismology, 12(1), 1–19. Retrieved from http://link.springer.com/10.1007/s10950-007-9067-x

Wathelet, M., Jongmans, D., Ohrnberger, M., & Bonnefoy-Claudet, S. (2008). Array performances for ambient vibrations on a shallow structure and consequences over Vs inversion. Journal of Seismology, 12(1), 1–19.